Low-velocity impacts into granular material: application to small-body landing

Naomi Murdoch[1]★, Melanie Drilleau[1]†, Cecily Sunday[1,2], Florian Thuillet[2],
Arnaud Wilhelm[1], Gautier Nguyen[1], Yves Gourinat[1]

[1]*Institut Supérieur de l'Aéronautique et de l'Espace (ISAE-SUPAERO), Université de Toulouse, 31400 Toulouse, France.*
[2]*Université Côte d'Azur, Observatoire de la Côte d'Azur, CNRS, Laboratoire Lagrange, Nice, 06304, France*

ABSTRACT

With the flourishing number of small body missions that involve surface interactions, understanding the mechanics of spacecraft - surface interactions is crucial for improving our knowledge about the landing phases of space missions, for preparing spacecraft operations, and for interpreting the results of measurements made during the surface interactions. Given their regolith-covered surfaces, the process of landing on a small body can be considered as an impact at low-velocity onto a granular material in reduced-gravity.

In order to study the influence of the surface material, projectile shape, and gravity on the collision dynamics we used two experimental configurations (one for terrestrial gravity experiments and one for reduced-gravity experiments) to perform low-velocity collisions into different types of granular materials: quartz sand, and two different sizes of glass beads (1.5 and 5 mm diameter). Both a spherical and a cubic projectile (with varying impact orientation) were used.

The experimental data support a drag model for the impact dynamics composed of both a hydrodynamic drag force and quasi-static resistance force. The hydrodynamic and quasi-static contributions are related to the material frictional properties, the projectile geometry, and the gravity.

The transition from a quasi-static to a hydrodynamical regime is shown to occur at lower impact velocities in reduced-gravity trials than in terrestrial gravity trials, indicating that regolith has a more fluid-like behaviour in low-gravity. The reduced quasi-static regime of a granular material under low-gravity conditions leads to a reduction in the strength, resulting in a decreased resistance to penetration and larger penetration depths.

Key words: minor planets, asteroids: general – comets: general – planets and satellites: surfaces

1 INTRODUCTION

The number of space missions involving an interaction between a probe and the surface of a small-body has flourished in recent years. Following in the footsteps of the JAXA *Hayabusa* asteroid sample return mission that returned samples of asteroid 25143 Itokawa to Earth in 2010 (Yoshimitsu et al. 2006; Tsuda et al. 2013), the *Hayabusa-2* mission successfully returned the first samples of primitive carbonaceous asteroid material to Earth on 5 December 2020. In addition to retrieving samples from the surface of asteroid 162173 Ryugu, the *Hayabusa-2* mission also deployed the *MINERVA and Mascot* surface packages to the surface of the asteroid

(Watanabe et al. 2017; Scholten et al. 2019), and performed an impact experiment using the *Small Carry-on Impactor* (Saiki et al. 2017; Arakawa et al. 2020).

In October 2020 NASA *OSIRIS-REX* mission (Lauretta et al. 2017) collected samples from the surface of another carbonaceous body, asteroid 101955 Bennu. During the spectacular Touch-And-Go sampling maneuver *OSIRIS-REX* collected a significant quantity of surface material that will be returned to Earth in 2023.

The upcoming DART (NASA) and Hera (ESA) planetary defense missions (launches planned for 2021 and 2024, respectively; Cheng et al. 2018b; Michel et al. 2018) to the binary asteroid 65803 Didymos, will also involve surface interactions. The DART mission will impact Dimorphos (the secondary component of the binary asteroid system) in order to perform the first demonstration of asteroid deflection by kinetic impact and the Hera mission will deploy

★ E-mail: naomi.murdoch@isae.fr
† E-mail: melanie.drilleau@isae.fr

small CubeSats that will land on Dimorphos (Michel et al. 2018; Van wal et al. 2020). Accelerometers are simple but powerful tools that can be used to record the acceleration profile during landing and rebounding of a surface package. The Hera Juventus CubeSat will include accelerometers in order to take measurements during the landing and to study the mechanical properties of asteroid Dimorphos.

Surface interactions will also be important for the JAXA Martian Moons eXploration (MMX) mission to Phobos, due for launch in 2024. The MMX mission will attempt to take a sample from the surface of Phobos to bring back to Earth (Campagnola et al. 2018). In addition, this mission will deploy a rover to the surface of Phobos that will be the first demonstration of locomotion on a regolith-covered, low-gravity planetary surface (Murdoch et al. 2020), and will provide an excellent opportunity for studying regolith dynamics on small body surfaces (Sunday et al. 2020a).

Despite the numerous successes described above, difficulties have also been encountered during the critical phase of landing or touching the surface of a small body, as demonstrated by the unintentional rebounding of *Philae* on the comet 67P/Churyumov-Gerasimenko in 2014 (Reinhard & Lars 2016; Basilevsky et al. 2016), and the failed landing of the *Hayabusa* surface package *MINERVA* (Biele et al. 2015).

One of the key areas in which we lack knowledge relevant to this specific mission stage is the behaviour of the surface material and its response during landing or other interactions such as sampling. Such an understanding is linked to the characteristics of the small body surface properties. Studying these interactions can also provide information about the small body surface material, as shown by Basilevsky et al. (2016). This knowledge is also crucial for investigating the evolution of small body surfaces and to better understand the main processes that have shaped the surfaces.

Recent investigations (both in-situ and from remote observations) have shown asteroids' surfaces to be composed of granular material known as regolith (for a review of asteroid surface geophysics see e.g., Murdoch et al. 2015). In the case of an asteroid landing, the small surface gravities and thus low escape velocities impose a low collision velocity of the lander with the surface in order to prevent the lander rebounding and escaping the gravitational field of the small body. Typical collision velocities for asteroid landers on space missions such as *Hayabusa-2* or *Hera* are on the order of tens of cm.s^{-1}. A simple description of the asteroid landing phase is thus a low-velocity impact of a projectile into a granular material under reduced-gravity conditions.

In this paper we start (Section 2) by presenting the current understanding of low velocity granular impacts and propose a theoretical model, based on previous work, to describe the peak acceleration, collision duration and penetration depth during the collisions. We then present (Section 3) the details of new experiments performed under both terrestrial and low-gravity in order to directly study the influence of target material, projectile shape and gravity on the collision dynamics. In Section 4 we present the results and compare the theoretical model predictions to the experimental data. Finally, Section 5 discusses the successes and limitations of the theoretical model the implications of our results for small bodies and small body missions.

2 LOW-VELOCITY GRANULAR IMPACTS

2.1 Previous low-velocity impact experiments

The diversity of the applications of low-velocity, shallow impacts results in contributions to this field from various domains including cratering, shock-absorption, planetary accretion or granular studies. This classical problem has been increasingly studied in previous years through theoretical (e.g., Allen et al. 1957; Ambroso et al. 2005b; Tsimring & Volfson 2005; Clark & Behringer 2013), numerical (e.g., Pica Ciamarra et al. 2004; Kondic et al. 2012; Clark et al. 2016; Cheng et al. 2018a) and experimental (e.g., Katsuragi & Durian 2007; Goldman & Umbanhowar 2008; Brzinski et al. 2013; Altshuler et al. 2014; Clark et al. 2015) methods. The main difficulty in the problem is that granular materials have the particularity of being capable of behaving as solids, fluids and gases at the same time. This makes it challenging to establish a reliable rheological model for the impacted material.

By performing direct measurements of the acceleration of projectiles impacting granular materials, previous studies reveal a universal scaling of the granular drag force applied by the material on the projectile during the collision (e.g., Katsuragi 2016). This drag force is composed of both a hydrodynamical (or inertial, rate-dominated) and a quasi-static (or frictional, rate-independent) contribution implying the existence of two collision regimes dominated by either hydrodynamical and or frictional forces depending on the projectile velocity and its depth within the material. Generally, at higher velocities, the collision will be in the hydrodynamical regime, while a quasi-static regime will be observed for lower velocities.

However, because the physics of such experiments must account for both fluid-like and solid-like behaviour during impact, the knowledge about the underlying physical mechanisms is still limited. Indeed, the studies cited above have opened a large set of questions, in particular concerning the role of the nature of the granular material, the projectile's shape, and the gravity level, on the force transmission.

In order to understand the nature of the force propagation into granular material during impact, Goldman & Umbanhowar (2008) used a variety of projectiles and granular materials to show the scaling of three key collision parameters as function of the collision velocities (for collision velocities > 1 m.s^{-1}). The maximal acceleration showed a quadratic dependence on the collision velocity, the collision final depth showed a linear dependence on the collision velocity, and the collision duration was found to be independent of the collision velocity.

Force transmission of granular impact was also explored by Clark et al. (2015), who performed experiments on photoelastic particles, showing that since grains near the free surface are uncompressed, force transmission during the first stage of collision in this region involves inherently nonlinear effects. A main result is that the force propagation occurs along complex, inhomogeneous force chains, and depends crucially on the inter-grain force law.

Among others, the role of the projectile's shape was investigated by Clark et al. (2014). Using projectiles with triangular noses, they systematically explored the effect of intruder shape on the collision process, and observed experimentally that momentum transfer per unit surface area is larger at the tip than elsewhere along the sides of the intruders.

Several studies also explored the role of the gravity level. In particular, using an Atwood Machine and numerical simulations, Goldman & Umbanhowar (2008) and Altshuler et al. (2014) investigated the influence of gravity on low speed granular impacts for an effective gravity between 1 and 9.81 m.s^{-2}. These reduced-gravity

experiments found the final maximum penetration depth to be independent of gravity. Using a specifically adapted drop tower (Sunday et al. 2016), Murdoch et al. (2017) investigated low speed granular collisions in lower gravity regimes (0.1 - 1 m.s^{-2}). Once again, the three scalings (the maximal acceleration, the collision final depth, and the collision duration) with collision velocity mentioned above were found to hold, even in the lower gravity regime. However, in this lower-gravity regime, the maximum penetration depth was found to increase with gravity; a different result to the experiments by Altshuler et al. (2014).

In the following, we will describe the dynamics of the projectile deceleration using a macroscopic force law, which relates the force exerted on the projectile by the granular material directly to the final penetration depth and the collision velocity. By analyzing the results of new experiments performed with different granular materials, projectile shape, and gravity levels, the primary goal of this work is to understand the conditions under which the considered force law is valid, and to connect this force law to a grain-scale description.

2.2 A theoretical model for low velocity impacts

Previous studies on experiments and simulations of low-velocity with granular media have mainly considered the depth to which an object penetrates before stopping. These studies have investigated how the penetration depth scales with various system parameters, and have demonstrated that the depth of penetration z_{stop} is found to scale as

$$z_{\text{stop}} \sim V_c^{\alpha_1} \frac{\rho_s}{\rho_g}^{\alpha_2} R^{\alpha_3}, \tag{1}$$

where V_c is the collision velocity of the spherical projectiles of radii R, ρ_s is the sphere density and ρ_g the granular particle density. There is no consensus on the values of the exponents α_1, α_2 and α_3. By performing experiments at low collision velocities (the maximum penetration depth was approximately a sphere diameter), Ambroso et al. (2005a,b) found $\alpha_1 = 2/3$, $\alpha_2 = 1/2$ and $\alpha_3 = 2/3$. Meanwhile Brisset et al. (2020) report $\alpha_1 = 1/2$, $\alpha_2 = 1/4$ and $\alpha_3 = 1/3$ for low-speed impacts into regolith simulant in microgravity conditions. Considering experiments at larger impact velocities and with projectile at higher density, a second study performed by de Bruyn & Walsh (2004) found a different scaling: $\alpha_1 = 1$, $\alpha_2 = \alpha_3 = 1/2$. Using two-dimensional disk simulations, Tsimring & Volfson (2005) found that $\alpha_1 = 4/5$, $\alpha_2 = 2/5$, and $\alpha_3 = 3/5$.

On the other hand, the experiments of Goldman & Umbanhowar (2008) demonstrated a linear scaling of penetration depth with impact velocity ($\alpha_1 = 1$). This linear scaling with impact velocity was also found in the numerical simulations of Pica Ciamarra et al. (2004). The different scaling relationships may be explained by the fact that the experiments fall into different scaling regimes, because they were performed using different projectile diameters and collision velocities (Ambroso et al. 2005a).

Considering the collision time, it has been found to be independent of the collision velocity for collision velocities higher than 1.5 m.s^{-1} (Pica Ciamarra et al. 2004; Goldman & Umbanhowar 2008), but for lower collision velocities, the collision duration increases with decreasing collision velocity (for a spherical projectile).

The precise empirical scaling of the penetration depth and the collision duration , and how exactly the exponents are related to the material properties, remains thus unclear. However, a consensus has emerged on the form of the resistive force that a granular bed exerts on a moving particle, enabling the estimation of the peak acceleration, the penetration depth and the collision duration, using

a unified force law. This unified force law is also directly linked to the material properties; an important consideration as our ultimate goal is to deduce the asteroid surface properties from measurements made during spacecraft-surface interactions.

Based on the phenomenological model proposed by Poncelet, most impact behaviour at low speed can be reconciled by a unified force law taking the form (e.g. Allen et al. 1957; Ambroso et al. 2005b; Tsimring & Volfson 2005; Katsuragi & Durian 2007; Goldman & Umbanhowar 2008; Umbanhowar & Goldman 2010; Pacheco-Vázquez et al. 2011):

$$F = mg - f(z) - h(z)v^2, \tag{2}$$

where m is the projectile mass, g is the gravitational acceleration, v the projectile velocity, and z the displacement of the lowest point on the projectile below the initial free surface of the grains. Equation 2 represents the stopping force due to granular media as the sum of the depth-dependent quasi-static resistance force $f(z)$ and the velocity-dependent inertial or hydrodynamic drag $h(z)$. The latter is conceptually the same force as the 'drag' used in fluid dynamics. When the external driving forces exceed the stationary condition, the individual grains lose the stationary state in their contacts and the granular material become fluidised.

With this approach, the resistance force model incorporates the solid-like and the fluid-like characteristics simultaneously. This force law is a nonlinear differential equation, and closed-form solutions of the dynamics can be typically obtained by making simplifying assumptions.

Following Katsuragi & Durian (2007), combining the equation 2 with the Newton's second law ($F = ma$), the acceleration a at a given fixed depth z_i should be quadratic in speed:

$$a = \frac{f(z_i)}{m} + \frac{h(z)}{m}v^2 - g. \tag{3}$$

Katsuragi & Durian (2007) has demonstrated that the projectile experiences a drag force $h(z)v^2$ that is independent of depth, thus we replace $h(z)$ by a constant term m/d_1, where d_1 is some characteristic length scale.

If we make the approximation of $f(z)$ as roughly constant (e.g. Allen et al. 1957; Goldman & Umbanhowar 2008; Umbanhowar & Goldman 2010; Clark & Behringer 2013; Bester & Behringer 2017), the acceleration peak at the impact can be expressed as:

$$a_{\text{peak}} = \frac{f_0}{m} + \frac{V_c^2}{d_1} - g, \tag{4}$$

where V_c is the measured collision velocity. In this formulation, the granular medium is modeled by a force law with a hydrodynamic drag term $1/d_1$ proportional to the square of the velocity (which dominates at high velocity), and a term f_0 that accounts for the quasi-static resistance force (which dominates for low velocity).

In order to obtain equations describing the maximum penetration depth z_{stop} and the collision duration t_{stop} as a function of V_c, using the two parameters f_0 and $1/d_1$, we follow the approach of Ambroso et al. (2005b) and Clark & Behringer (2013), by recasting the force law (equation 2) into an equation for the kinetic energy versus depth $K(z)$, assuming $K(z) = \frac{1}{2}mv^2$. The generalized drag force equation is thus rewritten:

$$\frac{dK}{dz} = mg - f_0 - \frac{2}{d_1}K. \tag{5}$$

This kinetic energy reformulation yields an inhomogeneous linear ordinary differential equation (ODE), by contrast to the nonlinear equation of motion (equation 2). The fact that equation 5 is a linear

ODE means that standard ODE methods immediately yield formal solutions for $K(z)$:

$$K(z) = K_P(z)(K_0 + \Phi(z)), \tag{6}$$

where K_0 is the kinetic energy at impact,

$$K_P(z) = \exp\left(\frac{-2z}{d_1}\right), \tag{7}$$

and

$$\Phi(z) = \frac{1}{2d_1}\left[\exp\left(\frac{2z}{d_1}\right) - 1\right](mg - f_0). \tag{8}$$

Substituting equations 7 and 8 in 6, it is possible to find the stopping distance by setting $K(z_{\text{stop}}) = 0$, yielding the stopping depth as a function of the impact energy K_0. The analytical expression of the maximum penetration depth z_{stop} is found to increase logarithmically with the collision velocity:

$$z_{\text{stop}} = \frac{d_1}{2}\ln\left[1 + \frac{mV_c^2}{d_1(f_0 - mg)}\right]. \tag{9}$$

Finally, the collision duration t_{stop} can be obtained by integrating the projectile acceleration (equation 2) for v between 0 and V_c:

$$t_{\text{stop}} = \frac{\text{atan}\left[V_c\sqrt{\frac{m}{d_1(f_0 - mg)}}\right]}{\sqrt{\frac{1}{d_1}\left(\frac{f_0}{m} - g\right)}}. \tag{10}$$

3 EXPERIMENTAL DESIGN AND DATA ANALYSIS

Two different types of experiments were performed in order to increase our understanding of the collision dynamics. First, experiments were performed under terrestrial gravity. Then, experiments were performed in reduced-gravity using the ISAE-SUPAERO specifically adapted drop tower facility (Sunday et al. 2016). Here we detail both experimental set-ups.

3.1 Experiments under terrestrial gravity

Figure 1 shows the experimental set-up used to perform low-velocity granular collisions under terrestrial gravity. The container, an aluminium bucket 35 cm in diameter was filled with 20 kg of granular material. The release mechanism for the impacting projectile is the same as in Murdoch et al. (2017): an electromagnet, controlled by a trigger wire, that is attached to a vertical rod allowing an adjustable drop height. The release mechanism is placed on top of the container and ensures the reproducibility of the drop height and thus the collision velocity. To further ensure the reproducibility of the trials, and to avoid any pre-compression effects (e.g., Bourrier et al. 2010), the granular bed is manually mixed and then smoothed using a brush before each collision experiment.

3.2 Experiments under reduced-gravity

The reduced-gravity experiments were performed using the ISAE-SUPAERO droptower facility described in detail in Sunday et al. (2016). Here the granular material (60 kg for the glass beads, 80 kg for the sand) is contained in a box that is 62 cm x 45 cm x 59 cm in size. Reduced-gravity is created by means of an Atwood machine: a system of pulleys and counterweights that allow a controlled,
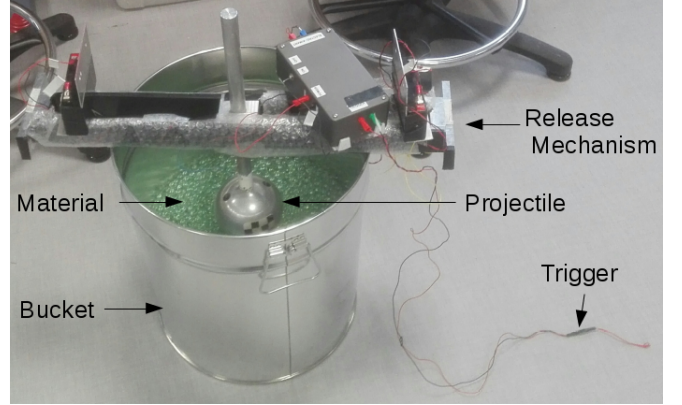

Figure 1. Terrestrial gravity trial configuration. An aluminium bucket (35 cm in diameter) is filled with the granular material (glass beads in this example). Before the experiment, a projectile (here an aluminium sphere) is attached to a release mechanism placed on top of the bucket. To perform the experiment the trigger wire is separated, and the projectile is automatically released from a controlled height (5 cm in this example).

constant downward acceleration of the container. Balancing the forces on the container and the counterweight, one can obtain the theoretical expression of the effective gravity experienced by the container (and thus the granular material):

$$g_{\text{eff}} = g - g\left(\frac{m_s - m_{cw}}{m_s + m_{cw}}\right), \tag{11}$$

where m_s is the container mass and m_{cw} is the total counterweight mass. Each counterweight can have a mass of between 0.5 and 5 kg (adjustable in 0.25 kg increments). This provides a theoretical range of effective gravities between 0.1 and $1\,m.s^{-2}$. However, in practice, effects such as rail friction lead to effective gravities slightly higher than these theoretical values (Murdoch et al. 2017).

3.3 Projectiles used in the experiments

Here we use the same 10 cm diameter 2017 aluminium sphere that was used in Murdoch et al. (2017). This projectile is designed to hold two wireless accelerometers (Section 3.4) and dimensioned to have a centred centre of mass for a total mass of 1 kg and a bulk density of 1909 kg.m^{-3}. In addition to this spherical projectile, we also use an aluminium cube (10 x 10 x 10 cm). A cubic shape was chosen as this is similar in shape to asteroid landers such as MASCOT (Jaumann et al. 2014). Just like the sphere, the cube has been designed to carry two accelerometers and to have the centre of mass as close to the geometrical centre as possible. The cube, however, has a bulk density of 753 kg.m^{-3}. Using different attachment points, the cube can be oriented to fall on a face or a corner. The two projectiles are shown in Fig. 2.

3.4 Sensors

During all trials, two YEI 3-space sensors [1] were mounted in the projectiles as shown in Fig. 3. These sensors include accelerometers that we used to measure the acceleration of the projectiles. In the

---

[1] Further information can be found in the User Manual accessible at https://yostlabs.com/wp/wp-content/downloads/3-Space/YEI_TSS_Users_Manual_3.0_r1_4Nov2014.pdf
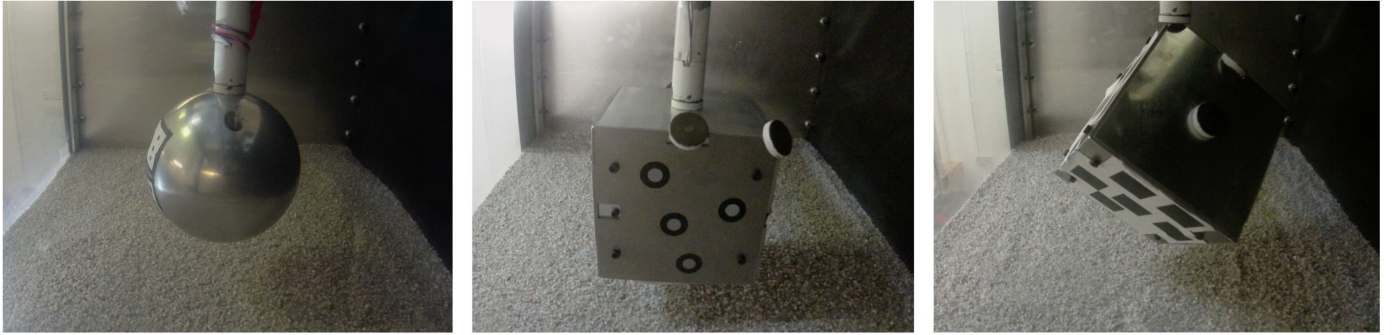
Figure 2. The projectiles used in the experiment. Left: Spherical projectile. Middle: Cubic projectile oriented to fall on a face. Right: Cubic projectile oriented to fall on an corner

.

low-gravity trials, at least one sensor was also attached to the surface container in order to provide an in-situ measurement of the effective gravity.

The main characteristics of the sensors can be found in Murdoch et al. (2017). No automatic filtering was used during the data acquisition, which allowed us to measure the projectile acceleration with the maximal sampling frequency of 1200 Hz. During the terrestrial gravity trials, the dynamic range of sensors was set to either $\pm 8g$ or $\pm 24g$, while the sensors were all set have a dynamic range of $\pm 8g$ in reduced-gravity.

3.5 Granular materials used in the experiments

Three different types of granular material were used in the experiments: quartz sand, and two different sizes of soda lime glass beads (SiLibeads Type M). The two kinds of glass beads are composed of the same material and, thus, only differ one from another in their particle diameters: 1.5 and 5 mm, respectively. The quartz sand, however, is much more angular than the spherical glass beads (Fig. 4). Table 1 provides some physical properties of these three granular materials. The bulk densities have been estimated by measuring the mass and volume of granular material in the containers. The angle of repose was measured by pouring the granular material through a funnel onto a horizontal surface.

3.6 Collision data analysis

The data from the sensors are synchronized by computing the normalised cross-correlation between the two sensors as described in Murdoch et al. (2017). For the terrestrial experiments, the experimental trials are then automatically identified in the accelerometer data via the detection of the free fall period (where the total measured acceleration falls below 0.1 m.s^{-2}). An example of such an analysis is shown in Fig. 5. Note that this figure shows the acceleration of the projectile, not the measured acceleration (a vertical accelerometer measures 9.8 m.s^{-2} at rest on Earth and 0 m.s^{-2} in free fall).

For each trial, the projectile velocity is computed by integrating the projectile acceleration from the moment the free fall is initiated. The collision velocity is defined as the velocity at the end of the free fall period, when projectile touches the granular surface and the collision starts. The penetration depth is then computed by integrating the projectile velocity from starting from the moment the collision starts. See Figure 5 for further explanation.

From these analyses, we can then obtain the three key parameters to describe the each collision experiment: the peak acceleration (a_{peak}), the final penetration depth (z_{stop}), and the collision duration (t_{stop}), in addition to the collision velocity (V_c).

For the trials in reduced-gravity the data analysis is similar to the terrestrial trials, with the main difference being that the relative motion of the projectile with respect to the granular surface is obtained using the sensors attached to the surface container (for full details see Murdoch et al. 2017).

Experiments have been performed varying the initial separation distance ('drop height' in the terrestrial gravity trials) between the projectile and the granular surface resulting in a range of collision velocities. For each collision experiment we performed the above analyses thus allowing us to investigate the evolution of the key collision parameters as a function of the collision velocity.

3.7 Analysis of boundary effects

The container sizes for both the terrestrial and low-gravity experiments were chosen to avoid any boundary effects (Katsuragi 2016; Nelson et al. 2008). Nonetheless, a set of experiments was performed under terrestrial gravity to verify that, indeed, no boundary effects were present. For this, the smallest container (the aluminium bucket) and the largest glass beads were used to give the smallest particle diameter to container diameter ratio used in our experiments. The container was filled with the glass beads to heights of 1 to 12 cm. The projectile was released, always from 5 cm above the granular surface, corresponding to the highest impact velocities during the trials. The impact accelerations were measured for each granular bed depth. The projectile bounced off of the bottom of the container for fill heights of 4 cm and less, but the projectile's peak acceleration and maximum penetration depth were more or less constant for fill heights exceeding 6 cm. The remainder of the experiments were performed with a fill height of 17 cm, or a height well over the threshold where boundary effects were observed in the experiment.

4 RESULTS

4.1 Validity of the theoretical model

First we investigate the validity of the theoretical model presented in Section 2.2 for an initial experimental configuration: the sphere impacting the quartz sand under terrestrial gravity.
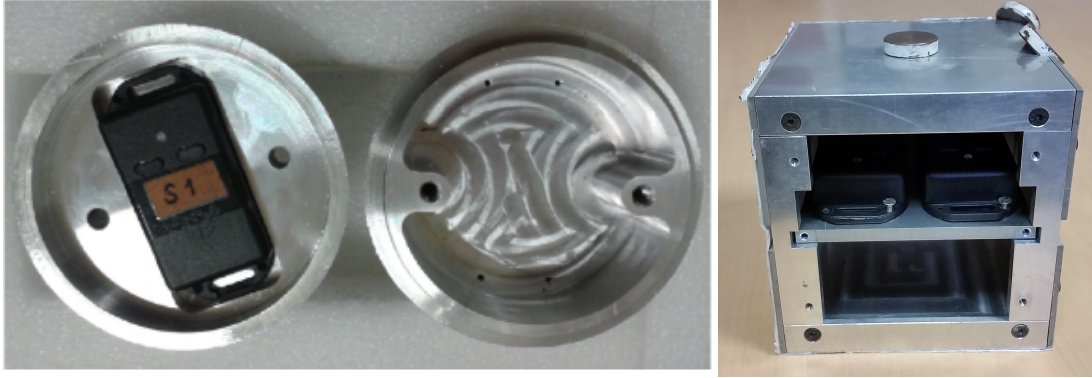
Figure 3. The sensors and the projectiles. Left: A YEI 3-Space sensor mounted in the spheric projectile. Right: two YEI 3-Space sensors mounted in the cubic projectile.

Table 1. Main mechanical properties of the granular materials used in the trials.

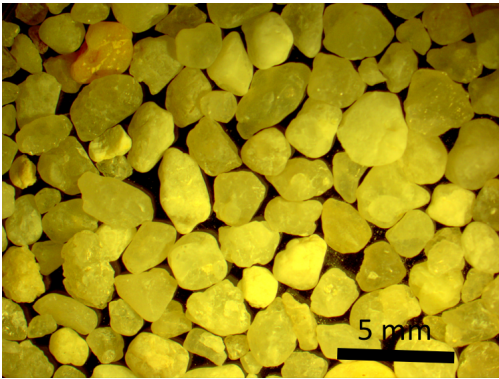| Material	Grain diameter (mm)	Bulk density for low-g trials (kg.m^{-3})	Bulk density for terrestrial trials (kg.m^{-3})	Angle of repose (deg)
Sand	1.83 (median)	1790	1798	37.4 ± 2.2
Soda lime glass	1.5	1520	1580	25.5 ± 1.6
Soda lime glass	5	-	1550	26.2± 2.5

Figure 4. An image taken of the quartz sand under a microscope. The grains are much more angular and irregular than the spherical glass beads.

The two characteristic parameters f_0 and $1/d_1$ from equation 4 are determined by fitting the peak accelerations as a function of the collision velocities, as shown in Figure 6a.

Using the least-square method, the intercept value obtained from the fit provides f_0, whereas the coefficient of the quadratic term gives $1/d_1$. The f_0 and $1/d_1$ values and their associated uncertainties (associated with the scatter in the experimental results) are provided in Table 2.

Having estimated the values of f_0 and $1/d_1$ from the quadratic fit to the measurements of a_{peak}, we use these values and equations 9 and 10 to provide theoretical expressions for the maximum penetration depth and collision duration as a function of the collision velocity.

The comparison between the predicted theoretical models, and the experimental data, is shown in Fig. 6 for the sphere impacting the quartz sand under terrestrial gravity. Taking into account the

uncertainties due to scatter in the experimental data, there is a relatively good agreement between the measured and predicted maximum penetration depth and collision duration and demonstrates the validity of our theoretical model.

Having demonstrated the validity of the theoretical model using the terrestrial trials with the spherical projectile falling in the quartz sand, in the following sections we consider how the collision dynamics are influenced by the surface material, the projectile geometry, and the gravity. For each experimental data set we apply the methodology presented above (that relies on the theoretical expressions detailed in Section 2.2) to determine the validity of the theoretical model for the various experimental configurations. This also allows us to analyse the influence of the surface material, the projectile geometry and the gravity on the quasi-static and hydrodynamic drag coefficients f_0 and $1/d_1$.

4.2 Influence of surface material

For all three surface materials tested (quartz sand, 1.5 mm and 5 mm glass beads; see Section 3.5), the peak acceleration scales quadratically with the collision velocity as expected from the theoretical model (Fig. 6a).

Following the same procedure as in Section 4.1, we first estimate the drag coefficients f_0 and $1/d_1$ for collisions into the 1.5 mm and 5 mm glass beads, and then we use these coefficients to predict a theoretical model for the final penetration depth and collision duration (Fig. 6b and c). Both the experimental measurements and the theoretical model results are shown in Fig. 6.

Concerning the 1.5 mm glass beads, the theoretical model predictions of the maximum penetration depth and the collision duration correctly reproduce the general trend of the experimental measurements, but there is a larger deviation between the theoretical model predictions and the measured data than for the quartz
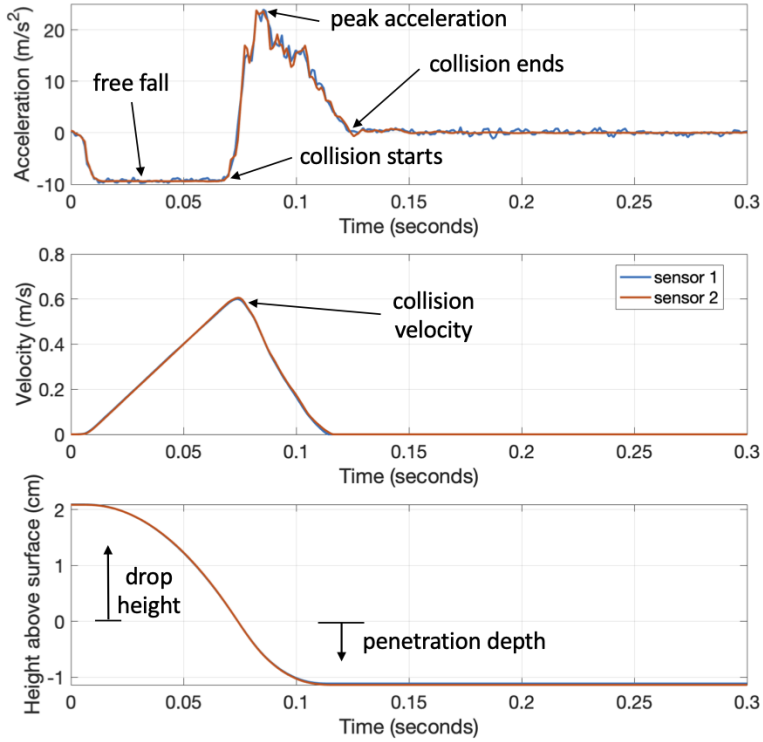
Figure 5. Example of terrestrial trial data analysis, considering a sphere impacting the quartz sand. Top: Acceleration of the projectile as a function of time during the experiment. Middle: Velocity of the projectile as a function of time during the experiment. Bottom: Vertical displacement of the projectile as a function of time during the collision. In each figure the data acquired by the two sensors inside the projectile is shown.

sand. In particular, the theoretical model underestimates the maximum penetration depth and overestimates the collision duration for collision velocities lower than 0.7 m.s^{-1}. The results for the 5 mm glass beads reveal a clear disagreement between the experimental data and the theoretical model predictions, with the model significantly underestimating both the maximum penetration depth and the collision duration.

Note that the independence of the collision duration on the collision velocity that was observed by Goldman & Umbanhowar (2008) for higher velocities (1-4 m.s^{-1}) is also observed here for the three different materials. However, this may be due to the lack of very low velocity collisions (< 0.4 m.s^{-1}) in our terrestrial gravity data set.

Looking at Table 1, the quartz sand and the 1.5 mm glass beads are similar in size, but differ principally in their frictional properties (angle of repose). The glass beads have a spherical particle shape with a small size distribution, while sand particles have irregular and variable particle shapes with a larger size distribution. This results in an increased bulk density and inter-particle friction for the sand with respect to the glass beads.

Comparing the drag parameters for these two materials then directly highlights the influence of these mechanical properties of the surface material on the drag coefficients. The values obtained for f_0 and $1/d_1$ for each of the different surface materials are in Table 2. The quasi-static resistance force term is slightly larger for the quartz sand (f_0 = 19±4 Nm) compared to the 1.5 mm glass beads (f_0 = 15±1 Nm) and the hydrodynamic drag force term ($1/d_1$) is significantly larger (34±6 m^{-1} and 12±1 m^{-1}, for the quartz sand and 1.5 mm glass beads, respectively), which means that this coefficient is strongly related to the frictional properties (and

bulk density) of the surface material. This implies that a granular material with more inter-particle friction generates more resistance to penetration (as would be expected). This can also be seen in Fig. 6; the projectile penetrates further into the glass beads and takes a longer time to come to rest that for the more frictional sand.

4.3 Influence of projectile geometry

To determine the influence of the projectile geometry on the three key collision parameters, we performed collisions using the quartz sand, and the different projectile shapes and orientations presented in Fig. 2: a spherical projectile, a cubic projectile oriented to fall on a face, and a cubic projectile oriented to fall on a corner. The two main differences between the spherical and cubic projectiles are their bulk density (equal to 1909 kg.m^{-3} and 753 kg.m^{-3} for the spherical projectile and the cubic projectile, respectively), and the contact area with the granular material.

As in the previous section where we varied the surface material (Section 4.2), the peak acceleration measured for each collision is fitted to a quadratic scaling for each of the projectiles to obtain the values of f_0 and $1/d_1$ coefficients. These values are then used to estimate the maximum penetration depth and the collision duration as a function of the collision velocity. The results of the measurements and the theoretical models are shown in Fig. 7.

We observe that, considering a similar surface material, the results highly depend on the size of the projectile's contact area with the granular material. Indeed, the cube oriented to fall on a corner penetrates the most easily, and the cube oriented to fall on a face meets with the largest resistance from the surface material.

In fact, the quasi-static resistance force is proportional to the
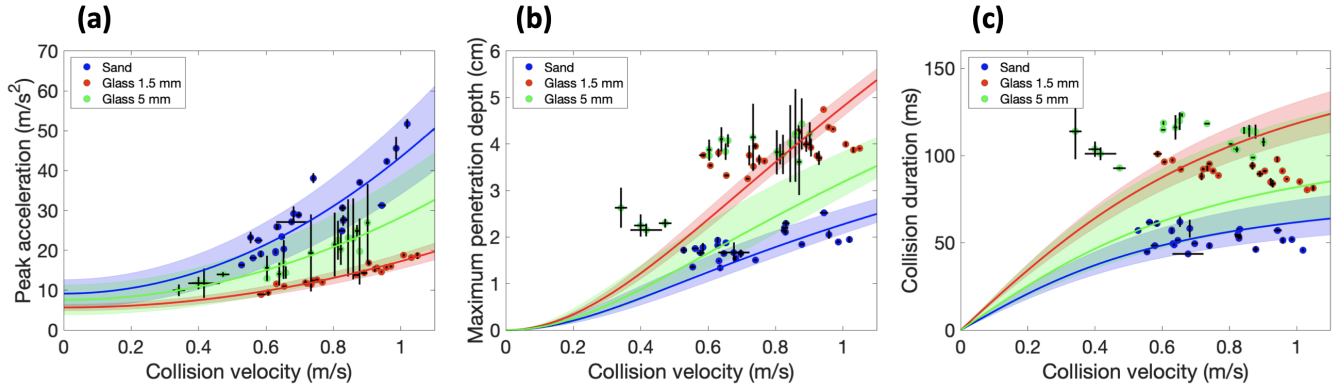
Figure 6. Evolution of the three key collision parameters with the collision velocity for the sphere impacting the quartz sand (blue), and for the 1.5 mm (red) and 5 mm (green) glass beads, under terrestrial gravity: (a) peak acceleration, (b) maximum penetration depth, and (c) collision duration. The black error bars show the standard deviation of measurements between the two sensors. The solid lines represent the theoretical expressions described in equations 4, 9, and 10. The coloured areas correspond to the 95% confidence bounds on the coefficients f_0 and $1/d_1$.

object's cross-section times the local pressure (Albert et al. 1999). Therefore, the large contact area of the cube face implies a larger resistance force exerted by the projectile on the granular material, explaining why the acceleration peak is larger, and the maximum penetration depth and the collision duration are smaller, compared to the sphere and the cube falling on a corner. The cubic projectile falling on the face is prevented from penetrating the material due to the quasi-static resistance force, leading to a much larger f_0 coefficient (f_0=61±7 Nm, Table 2) compared to the sphere (f_0=19±4 Nm).

The theoretical model can be fit to the peak accelerations for all projectile forms but the theoretical model fails to describe the experimental data for the cube falling on a corner, by largely under-estimating both the maximum penetration depth and the collision velocity.

4.4 Influence of reduced-gravity

Trials in reduced-gravity were performed using the experiment configuration described in Section 3.2. Previous investigations using the spherical projectile and the quartz sand have shown that the peak acceleration during a collision follows a quadratic scaling with collision velocity, even in the reduced-gravity (0.1 - 1 m.s^{-2}) regime (Murdoch et al. 2017). Here, we perform additional reduced-gravity trials of the sphere impacting the quartz sand in order to verify this result and investigate in further detail the influence of the gravity on the drag coefficients (f_0, $1/d_1$).

In order to explore the influence of the nature of the granular surface, we also conduct reduced-gravity trials of the sphere impacting the 1.5 mm glass beads. Specifically, we performed trials for effective gravities between 0.4 and 1.4 m.s^{-2} for the quartz sand, and between 1.15 and 1.21 m.s^{-2} for the 1.5 mm glass beads.

The results are shown in Fig.8 and Fig.9 for the two different surface materials. Again, the quadratic fit to the peak acceleration is used to obtain the two drag coefficients and these are reported in Table 2.

Unfortunately, due to the experimental limitations, there are no experimental data available for the same collision velocity at different gravity levels. Therefore, we rely on the fits to the theoretical model to extrapolate the experimental data for the two regimes.

For the two types of granular material, the same behaviour is

observed in reduced-gravity with respect to terrestrial gravity (Fig.8 and Fig.9). For low collision velocities, the quadratic fits imply that the peak acceleration is lower in reduced-gravity compared to terrestrial gravity. Then, above a certain collision velocity (around 0.4 m.s^{-1} for quartz sand and 1 m.s^{-1} for 1.5 mm glass beads) the quadratic fits predict a higher peak acceleration in reduced-gravity than in terrestrial gravity. This behaviour needs to be confirmed with further data in the future.

It can be seen also that the reduced-gravity trials show larger penetrations depths and longer collision durations compared to the terrestrial gravity trials. The theoretical model provides a reasonable estimation for the penetration depth but cannot explain the collision duration in reduced-gravity; the collision durations, particularly at the lowest collision velocities, are significantly underestimated by the model.

Our results indicate a clear increase of the hydrodynamic drag term $1/d_1$ in reduced-gravity (Table 2), with values equal to 76±10 m^{-1} in reduced-gravity compared to 34±6 m^{-1} in terrestrial gravity for the quartz sand, and with values equal to 17±7 m^{-1} in reduced-gravity compared to 12±1 m^{-1} in terrestrial gravity for the 1.5 mm glass beads.

On the contrary, the quasi-static resistance force term f_0 decreases with decreasing gravity, with values equal to 2.3±0.5 Nm and 2.2±0.5 Nm for the quartz sand and the 1.5 mm glass beads in reduced-gravity, whereas the values in terrestrial gravity are equal to 19±4 Nm for the quartz sand and 15±1 Nm for the 1.5 mm glass beads.

These significant differences between the $1/d_1$ and f_0 values in the different gravity regimes suggest that the frictional interactions in the quasi-static regime have a reduced importance whereas the hydrodynamic drag becomes much more important in low-gravity.

5 DISCUSSION

5.1 Limitations of the theoretical model

We find that the peak accelerations in all experiments (all surface materials, projectile forms and gravity levels) can be reasonably described with the proposed theoretical model (Section 2.2). However, additional experimental data at larger ranges of collision velocities
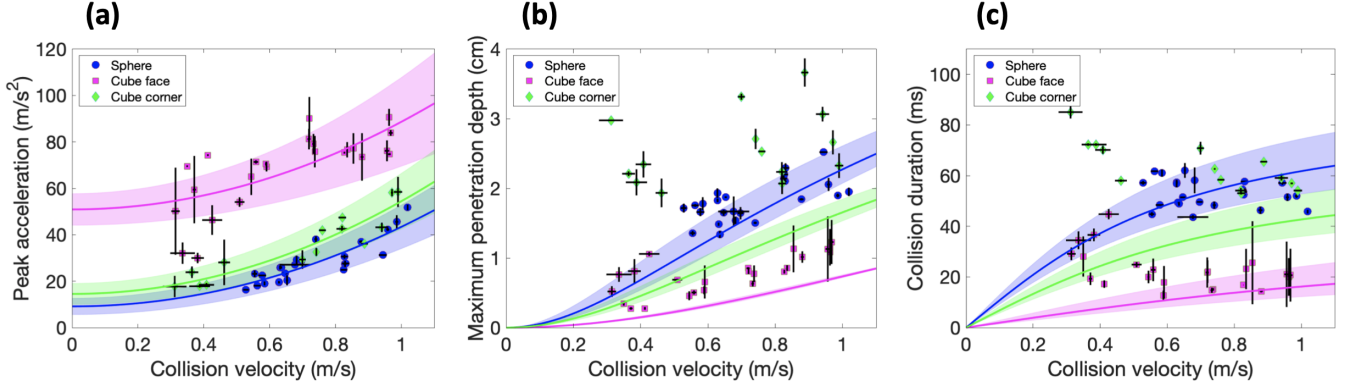
Figure 7. Evolution of the three key collision parameters with the collision velocity for different projectiles impacting the quartz sand, under terrestrial gravity: (a) peak acceleration, (b) maximum penetration depth, and (c) collision duration. The measurements using a spherical projectile, a cube falling on a face, and a cube falling on a corner, are displayed in blue, pink, and green, respectively. The black error bars show the standard deviation of measurements between the two sensors. The solid lines represent the theoretical expressions described in equations 4, 9, and 10. The blue areas correspond to the 95% confidence bounds on the coefficients f_0 and $1/d_1$.
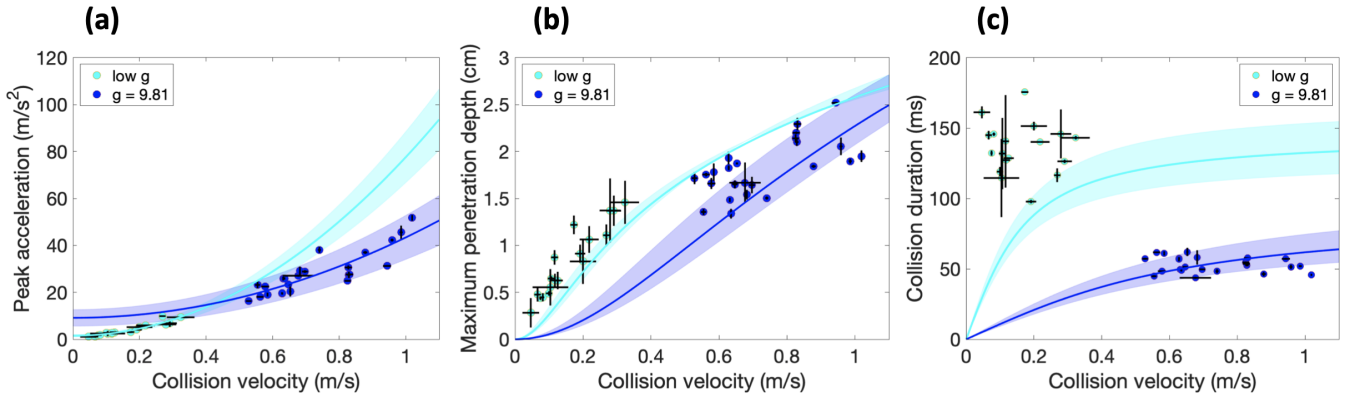

Figure 8. Evolution of the three key collision parameters with the collision velocity for the sphere impacting the quartz sand, under terrestrial gravity (blue) and low-gravity (light blue): (a) peak acceleration, (b) maximum penetration depth, and (c) collision duration. The trials performed with the drop tower have an effective gravity ranging from 0.4 to 1.4 m.s^{-2}. The black error bars show the standard deviation of measurements between the two sensors. The solid lines represent the theoretical expressions described in equations 4, 9, and 10. The coloured areas correspond to the 95% confidence bounds on the coefficients f_0 and $1/d_1$.

Table 2. Main collision properties of the different collision configurations. $1/d_1$ refers to the hydrodynamic drag term and f_0 is the quasi-static resistance force term.

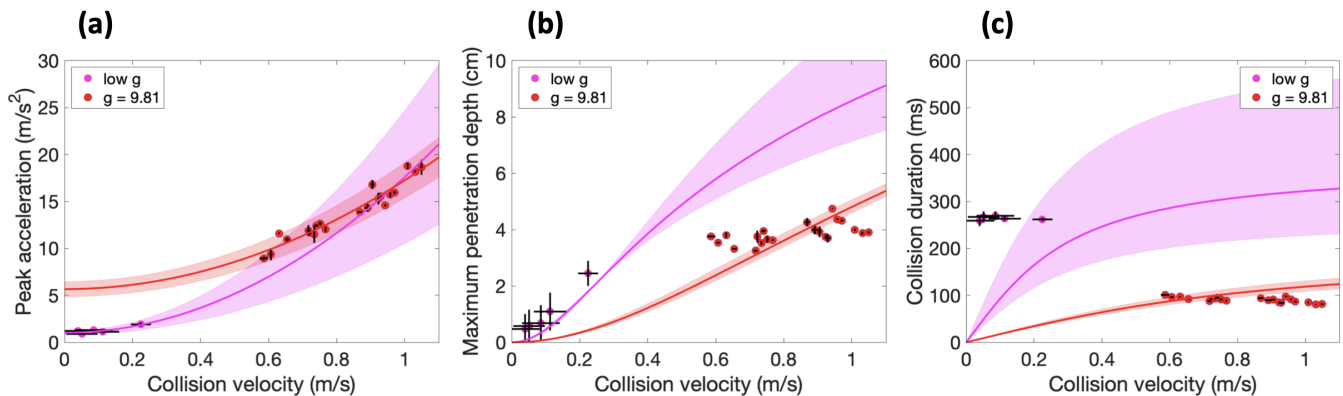| Material	Projectile	Effective gravity $(m.s^{-2})$	$1/d_1 (m^{-1})$	$f_0 (Nm)$
Quartz Sand	Sphere	9.81	34±6	19±4
1.5 mm Glass Beads	Sphere	9.81	12±1	15±1
Quartz Sand	Cube Face	9.81	38±12	61±7
Quartz Sand	Sphere	0.4 - 1.4	76±10	2.3±0.5
1.5 mm Glass Beads	Sphere	1.15 - 1.21	17±7	2.2±0.2

Figure 9. Evolution of the three key collision parameters with the collision velocity for the sphere impacting the 1.5 mm glass beads, under terrestrial gravity (red) and low-gravity (pink): (a) peak acceleration, (b) maximum penetration depth, and (c) collision duration. The trials realized with the drop tower has an effective gravity ranging from 1.15 to 1.21 m.s^{-2}. The black error bars show the standard deviation of measurements between the two sensors. The solid lines represent the theoretical expressions described in equations 4, 9, and 10. The coloured areas correspond to the 95% confidence bounds on the coefficients f_0 and $1/d_1$.

would be very useful to verify the model validity over a larger range of impact velocities.

Nonetheless, although the peak accelerations can be well described by the theoretical model, there are limitations with respect to the capability of the model to accurately predict the penetration depth and collision duration in certain situations.

Specifically, as the particle size increases, the theoretical model breaks down. The differences between the experimental data and the model predictions indicate that the theoretical model seems to be reasonable for smaller particles but becomes inappropriate for larger particles, thus implying that the model breaks down when the particles can no longer be treated as a continuum with respect to the projectile.

Issues also arise for certain projectile forms. In general, a projectile slows down due to forces exerted normally on the projectile by the surrounding grain network. Contrary to the sphere and the cube falling on a face, for the collisions with the cube corner, the surface in contact with the quartz sand rapidly changes when the collision occurs, as the corner penetrates into the granular surface.

In the theory considered here (Section 2.2), the variation of the projectile's contact surface, and consequently the variation of the force with the penetration depth is not taken into account. This oversimplification of the theoretical model may explain the divergence between the experimental data for the cube impacting on a corner and the theoretical model.

Indeed, Tsimring & Volfson (2005) argued that the form of $f(z)$ should vary from quadratic to constant due to the shapes of the projectile and of the growing crater excavated by its motion. Similarly, Brzinski et al. (2013) suggested the quasi-static resistance force term has a strong dependence on projectile shape, especially while the projectile is only partially submerged, as it the case for the cube falling on the corner. Another example is the measurements by Goldman & Umbanhowar (2008) that have shown a substantial offset term once the projectile is fully submerged, $f(z) = f_0 + kz$.

With regards to the reduced-gravity experiments - the peak accelerations can be correctly modelled with the proposed theoretical model, and the model provides reasonable predictions for the maximum penetration depth. However, the collision duration, particularly at the lowest collision velocities, are significantly underestimated by the current model. This implies that the theoretical model needs to be improved in order to correctly capture the dynamics of low-velocity impacts in reduced-gravity. In addition, the assumption that the quasi-static resistance term, f_0, is constant is likely to lead to larger inaccuracies in the theoretical model for the lower collision velocities. Given that the reduced-gravity trials are also in a lower range of collision velocities, this model simplification may disproportionately affect the reduced-gravity trials leading to the larger discrepancies between the theoretical and observed collision duration Figs. 8-9).

The experimental measurements of the cube falling on a corner and the reduced-gravity experiments may, therefore, be better explained by depth-dependent laws that describe the forces during impact, and such an improvement should be considered in the future. For example Goldman & Umbanhowar (2008); Brzinski et al. (2013) vary the quasi-static resistance force term $f(z)$ as a function of depth, instead of considering it to be constant. Instead of considering that they are constant, $f(z)$ and $h(z)$ (see Eq. 3) could be measured experimentally, as detailed by Clark & Behringer (2013) and Bester & Behringer (2017), using the velocity and depth measurements as a function of time for each trial. This method has the advantage to provide no assumptions about the functional form of $f(z)$ and $h(z)$.

These model improvements may help to account for both the projectile shape variation and the model behaviour at low-gravity and could also improve the very low velocity model results; the current theoretical model predicts zero penetration depth and zero collision duration for a null collision velocity, whereas a finite penetration and duration are always observed in the experimental data even for the lowest collision velocities.

Another model assumption that could be questioned is the use of the peak acceleration in the force law formulation (equation 4). As described in Goldman & Umbanhowar (2008), there are significant fluctuations in the acceleration profile during impact. These fluctuations depend on the characteristics of the material being penetrated and are not yet described by any existing models of impact. In the case of large fluctuations in acceleration, this may result in inaccuracies in the determination of the drag force parameters f_0 and d_1.

Ideally, these results should be further investigated for even lower collision velocities (<0.5 m.s^{-1}) under terrestrial gravity in

order to complete the theoretical model by giving the penetration depth for very small and null collision velocities. However, with our current experimental configuration it is difficult to both achieve such small collision velocities and obtain reliable measurements for such short duration experiments. Similarly, it would be valuable to have reduced-gravity impact experiments at higher collision velocities (>0.4 m.s^{-1}) in order to directly compare the influence of gravity for otherwise identical impact experiments. Again, however, we are limited by the capabilities (and drop time) available in the current drop tower facility (Sunday et al. 2016).

Additional experiments or numerical simulations (e.g. Sunday et al. 2020b; Schwartz et al. 2012) that allow effective gravities between 1 m.s^{-2} and 9.81 m.s^{-2} would further improve our understanding of the influence of gravity on the various regime changes. Similarly, impact data with effective gravities <0.2 m.s^{-2} would be extremely useful in order to probe the behaviour of regolith in the limit of zero gravity.

Experiments with impact velocities ranging from 0.01 to 2.3 m.s^{-1} have been performed in low-gravity using parabolic flights, a drop-tower and the ISS (Colwell & Taylor 1999; Colwell 2003; Colwell et al. 2008; Brisset et al. 2018, 2020). There were no in-situ acceleration measurements during the impacts so the data cannot be used for the analyses presented here. Nonetheless, different responses of the regolith, such as the quantity and velocity of ejecta, where observed in low gravity conditions for impact speeds above and below a threshold of 0.2-0.4 m.s^{-1} (Colwell 2003; Brisset et al. 2020).

In addition to investigation a depth-dependent theoretical model in the future (e.g., Goldman & Umbanhowar 2008; Brzinski et al. 2013; Clark & Behringer 2013; Bester & Behringer 2017), interesting future work will be to consider how this theoretical model applies to oblique impacts and for collisions involving rebounds. For example, Wright et al. (2020) perform experiments of low velocity oblique impacts of spherical projectiles into a fine sand (under terrestrial gravity). They find that a single force law does not fit both the penetration and rebound phases of the trajectories. Therefore, for higher speed impacts, where rebounds occur, the theoretical model used here may need to be further revised.

5.2 Consequences for small bodies

Knowledge of the mechanical properties of regolith are important for understanding the evolution of small body surfaces, and for the design of future space missions that plan to interact with the regolith directly. Data recorded by an onboard accelerometer (and, ideally, a gyroscope in order to determine the impact orientation) during the landing phase of a small body surface package could be an opportunity to study the mechanical properties of the impacted regolith (e.g., Bernauer et al. 2020). Indeed, in the context of a small-body landing, the surface gravity, the impact velocity, and the impacting projectile geometry will likely be known. Images of the touchdown location would also provide information about the regolith particle size. Consequently, one could potentially use the measurements of the different collision parameters, a_{peak}, z_{stop} and t_{stop} to estimate the regolith frictional properties. In addition, any discontinuities in the acceleration profile during the collision will be indicative of a layering or heterogeneous surface material, whereas a smooth acceleration profile will be more indicative of a continuous, homogeneous surface material.

As described in the theoretical model (Section 2.2), and as it has been confirmed by our experimental measurements (Section 4), there exist two regimes during a granular impact: a quasi-static (rate-independent) regime at low impact velocities, and a hydrodynamic (rate-dependent) regime at higher velocities.

We find that for the collision velocities investigated here (< 1 m.s^{-1}), the maximum penetration depth increases as gravity decreases. However, the penetration depth is also influenced by the properties of the surface material with more angular particles generating more resistance to penetration. Consequently, in order to model a low-velocity asteroid landing we need to account for both the increased resistance due to the interlocking of highly angular particles (e.g., Tsuchiyama et al. 2011), and the decreased resistance to penetration due to the (almost) absence of the quasi-static regime.

The most angular granular material used in these experiments - quartz sand - remains significantly more rounded than asteroidal regolith. Further experiments (using, for example asteroid or lunar regolith simulant), or numerical simulations, would be necessary to quantify the competing effects of increased angularity and decreased gravity.

Theoretically speaking, the impact velocity at which an impact transitions from the quasi-static regime to the hydrodynamical regime can be seen as the velocity $V_{transition}$ such that:

$$\frac{V_{transition}^2}{d_1} > \frac{f_0}{m}. \tag{12}$$

Thus,

$$V_{transition} = \sqrt{\frac{d_1 f_0}{m}}. \tag{13}$$

The significant differences between the quasi-static resistance force coefficient (f_0), and the hydrodynamic drag coefficient ($1/d_1$) in the different gravity regimes suggest that the quasi-static frictional interactions have a reduced importance whereas the hydrodynamic drag becomes much more important in low-gravity conditions. Indeed, the experimental results for the spherical projectile impacting the quartz sand demonstrate that the transition velocity decreases as the gravitational acceleration decreases ($V_{transition} = 0.75$ m.s^{-1} for the terrestrial gravity experiments and $V_{transition} = 0.17$ m.s^{-1} in reduced-gravity). In the case of the low surface gravity of a small body, the transition from the hydrodynamical regime to the quasi-static regime will then occur at much lower impact velocities than on Earth. In other words, the low-gravity environment makes a granular surface material more likely to behave like a fluid, confirming the previous hypothesis of (Murdoch et al. 2017).

The smallest effective gravity obtained in our experiments is just less than that of asteroids (1) Ceres and (4) Vesta (Carry et al. 2007; Russell et al. 2012). However, this is still several orders of magnitude larger than the surface gravity of truly small bodies. Indeed, if we consider the case of zero gravity, and assuming that there is no confining pressure, the quasi-static regime should not exist. The only existing stress scale should be the kinetic pressure (ρV^2), arising from the collision processes (Katsuragi & Durian 2007; Seguin, A. et al. 2016).

In the absence of the quasi-static regime, the strength of the surface material is significantly reduced. Following the *Hayabusa-2 Small Carry-on Impactor* experiment, Arakawa et al. (2020) conclude that, surprisingly, the crater was formed in the gravity-dominated regime on the surface of the small (< 1 km diameter) asteroid (162173) Ryugu. We suggest that the reduced strength of the surface material, due specifically to the low-gravity environment, is an explanation for this unexpected behaviour. Additionally, the reduced quasi-static regime may also explain the very small re-

sistive force encountered by the *OSIRIS-REX* spacecraft during the sampling of the even smaller ($\sim$ 500 m) asteroid (101955) Bennu [2].

6   CONCLUSIONS

Using two different experimental set-ups, including a drop tower facility (Sunday et al. 2016), low-velocity collision trials into granular material were performed in terrestrial gravity, and reduced-gravity (0.15 - 1.4 g). This corresponds to a lower gravity regime than those investigated by Altshuler et al. (2014), but similar to the experiments of Murdoch et al. (2017). The collision experiments were performed using quartz sand (average grain size of 1.8 mm) and soda lime glass beads of particle size 1.5, and 5 mm as surface materials, and with two different projectiles: an aluminium sphere and an aluminium cube. The latter can be oriented to fall either on a face or a corner.

Using data obtained from in-situ accelerometers, the collision dynamics were studied, with particular attention being given to how the following three key collision parameters vary with the collision velocity: the peak acceleration, the final penetration depth and the collision duration.

Using the data obtained from the collisions of the spherical projectile impacting the quartz sand under terrestrial gravity, we validate an analytical model linking the peak acceleration, the final penetration depth, and the collision duration to the collision velocity. The analytical model assumes that the total force exerted by the material on the projectile is composed of both a quasi-static resistance force term and a hydrodynamical drag force term that are quantified by their respective coefficients: f_0 and $1/d_1$.

The collision experiments under terrestrial gravity for the sphere impacting the two different sizes of glass beads then served both to investigate the influence of the impacted material on our two drag coefficients, and to explore the limits of validity of the analytical model. The theoretical model shows a reasonably good fit to the data obtained with quartz sand and 1.5 mm glass beads. However, the model fails to explain the 5 mm glass beads data, probably because the model breaks down when the particles can no longer be treated as a continuum with respect to the projectile.

Both the quasi-static resistance force term (f_0) and the hydrodynamical drag force term ($1/d_1$) are larger for the quartz sand compared to the 1.5 mm glass beads, implying that a granular material with more inter-particle friction generates more resistance (as would be expected).

The use of different projectiles (a sphere, a cube falling on a face, and a cube falling on a corner) allowed an initial investigation of the influence of the contact area between the projectile and the granular surface. The theoretical model is able to reproduce the key parameters for the sphere and the cube falling on a face. However, as we have no depth dependence in the theoretical model, it is not adapted to explain the trials of the cube falling on a corner in which the surface of contact with the granular material rapidly changes during the collision.

Finally, our drop tower facility permitted a more detailed investigation of the role of gravity on the collision parameters during a granular impact, and the influence of the gravity on the drag coefficients for the quartz sand and the 1.5 mm glass beads. The trials under reduced-gravity demonstrated clear differences compared to those performed under terrestrial gravity: specifically, the reduced-gravity trials show smaller acceleration peaks at low velocity collision, compared to the results at terrestrial gravity. Additionally, both the maximum penetration depth and the collision duration increase in reduced-gravity. Our results, showing an increase of the hydrodynamic drag term ($1/d_0$) and a decrease of the quasi-static resistance term (f_0) in reduced-gravity, indicate that the surface regolith is expected to present less resistance and exhibit a more fluid-like behaviour in reduced-gravity, as previously suggested by (Murdoch et al. 2017, 2013).

The reduced strength of the asteroid surface material, due specifically to the absence of the quasi-static regime in the low-gravity environment, may also explain why the *Hayabusa-2 Small Carry-on Impactor* crater formed in a gravity-dominated regime on the asteroid (162173) Ryugu (Arakawa et al. 2020), and why the *OSIRIS-REX* spacecraft encountered very little resistance from the surface of asteroid (101955) Bennu.

In preparation for future missions such as Hera (Michel et al. 2020), further studies will also be performed focussing on the interpretation of accelerometer data during individual collisions, in addition to the data from an ensemble of experiments as described in this paper.

DATA AVAILABILITY

The data underlying this article will be shared on reasonable request to the corresponding authors.

---

[2] https://www.planetary.org/planetary-radio/1028-2020-dante-lauretta-osiris-rex

REFERENCES

Albert R., Pfeifer M. A., Barabási A.-L., Schiffer P., 1999, Phys. Rev. Lett., 82, 205

Allen W. A., Mayfield E. B., Morrison H. L., 1957, Journal of Applied Physics, 28, 370

Altshuler E., Torres H., González-Pita A., Sánchez-Colina G., Pérez-Penichet C., Waitukaitis S., Hidalgo R. C., 2014, Geopysical Research Letters, 41, 3032

Ambroso M. A., Santore C. R., Abate A. R., Durian D. J., 2005a, Phys. Rev. E, 71, 051305

Ambroso M. A., Kamien R. D., Durian D. J., 2005b, Phys. Rev. E, 72, 041305

Arakawa M., et al., 2020, Science, 368, 67

Basilevsky A. T., Krasil'nikov S. S., Shiryaev A. A., Mall U., Keller H. U., Skorov Y. V., Mottola S., Hviid S. F., 2016, Solar System Research, 50, 225

Bernauer F., R.F. G., Murdoch N., Dehant V., Sollberger D., 2020, In Press, Earth, Planets and Space

Bester C. S., Behringer R. P., 2017, Phys. Rev. E, 95, 032906

Biele J., et al., 2015, in Spacecraft Reconnaissance of Asteroid and Comet Interiors. p. 6002

Bourrier F., Nicot F., Darve F., 2010, Comptes Rendus Mecanique, 338, 639

Brisset J., Colwell J., Dove A., Abukhalil S., Cox C., Mohammed N., 2018, Progress in Earth and Planetary Science, 5, 73

Brisset J., Cox C., Anderson S., Hatchitt J., Madison A., Mendonca M., Partida A., Remie D., 2020, A&A, 642, A198

Brzinski T. A., Mayor P., Durian D. J., 2013, Physical Review Letters, 111

Campagnola S., Yam C. H., Tsuda Y., Ogawa N., Kawakatsu Y., 2018, Acta Astronautica, 146, 409

Carry B., Dumas C., Fulchignoni M., Merline W. J., Berthier J., Hestroffer D., Fusco T., Tamblyn P., 2007, Astronomy & Astrophysics, 478, 235–244

Cheng B., Yu Y., Baoyin H., 2018a, Physical Review E, 98

Cheng A. F., et al., 2018b, Planetary and Space Science, 157, 104

Clark A. H., Behringer R. P., 2013, EPL (Europhysics Letters), 101, 64001

Clark A. H., Petersen A. J., Behringer R. P., 2014, Physical Review E, 89, 012201

Clark A. H., Petersen A. J., Kondic L., Behringer R. P., 2015, Physical Review Letters, 114, 144502

Clark A. H., Kondic L., Behringer R. P., 2016, Physical Review E, 93, 050901

Colwell J. E., 2003, Icarus, 164, 188

Colwell J. E., Taylor M., 1999, Icarus, 138, 241

Colwell J. E., et al., 2008, Icarus, 195, 908

Goldman D. I., Umbanhowar P., 2008, Physical Review E, 77, 021308

Jaumann R., et al., 2014, in Lunar and Planetary Science Conference. p. 1817

Katsuragi H., 2016, Physics of Soft Impact and Cratering, 1 edn. Lecture Notes in Physics 910, Springer Japan, http://gen.lib.rus.ec/book/index.php?md5=AC67000036F5CDFE9B8691653278BBE5

Katsuragi H., Durian D. J., 2007, Nature Physics, 3, 420

Kondic L., Fang X., Losert W., O'Hern C., Behringer R., 2012, Physical review. E, Statistical, nonlinear, and soft matter physics, 85, 011305

Lauretta D. S., et al., 2017, Space Science Reviews, 212, 925

Michel P., et al., 2018, Advances in Space Research, 62, 2261

Michel P., Falke A., Ulamec S., The NEO-MAPP team 2020, in EPSC Joint Meeting 2020. pp EPSC2020–103

Murdoch N., Rozitis B., Green S. F., Michel P., de Lophem T.-L., Losert W., 2013, Monthly Notices of the Royal Astronomical Society

Murdoch N., Sánchez P., Schwartz S., Miyamoto H., 2015, Asteroid Surface Geophysics. University of Arizona Press

Murdoch N., Avila Martinez I., Sunday C., Zenou E., Cherrier O., Cadu A., Gourinat Y., 2017, Monthly Notices of the Royal Astronomical Society

Murdoch N., et al., 2020, in European Planetary Science Congress. pp EPSC2020–247

Nelson E., Katsuragi H., Mayor P., Durian D. J., 2008, Physical review letters, 101, 068001

Pacheco-Vázquez F., Caballero-Robledo G., Solano-Altamirano J., Altshuler E., Batista-Leyva A. J., Ruiz-Suárez J., 2011, Physical review letters, 106, 218001

Pica Ciamarra M., Lara A. H., Lee A. T., Goldman D. I., Vishik I., Swinney H. L., 2004, Physical Review Letters, 92

Reinhard R., Lars W., 2016, Planetary and Space science, 125, 12

Russell C. T., et al., 2012, Science, 336, 684

Saiki T., et al., 2017, Space Science Reviews, 208, 165

Scholten F., et al., 2019, Astronomy & Astrophysics, 632, L3

Schwartz S. R., Richardson D. C., Michel P., 2012, Granular Matter, 14, 363

Seguin, A. Lefebvre-Lepot, A. Faure, S. Gondret, P. 2016, Eur. Phys. J. E, 39, 63

Sunday C., et al., 2016, Review of Scientific Instruments, 87

Sunday C., Murdoch N., Tardivel S., Imperatore N., Michel P., Ulmec S., 2020a, in European Planetary Science Congress. pp EPSC2020–234

Sunday C., Murdoch N., Tardivel S., Schwartz S. R., Michel P., 2020b, Monthly Notices of the Royal Astronomical Society, 498, 1062

Tsimring L. S., Volfson D., 2005, in Powders and Grains.

Tsuchiyama A., et al., 2011, Science, 333, 1125

Tsuda Y., Yoshikawa M., Abe M., Minamino H., Nakazawa S., 2013, Acta Astronautica, 91, 356

Umbanhowar P., Goldman D. I., 2010, Phys. Rev. E, 82, 010301

Van wal S., Karatekin O., Moreno Villa V. M., Goldberg H., 2020, in European Planetary Science Congress. pp EPSC2020–683

Watanabe S.-i., Tsuda Y., Yoshikawa M., Tanaka S., Saiki T., Nakazawa S., 2017, Space Science Reviews, 208, 3

Wright E., et al., 2020, Icarus, 351, 113963

Yoshimitsu T., Kubota T., Nakatani I., 2006, in 36th COSPAR Scientific Assembly.

de Bruyn J. R., Walsh A. M., 2004, Canadian Journal of Physics, 82, 439